Article

Electroporation of DC-3F Cells Is a Dual Process

Lars H. Wegner,[1,*] Wolfgang Frey,[1] and Aude Silve[1]
[1]Karlsruhe Institute of Technology, Institute for Pulsed Power and Microwave Technology (IHM), Campus North, Eggenstein-Leopoldshafen, Germany

ABSTRACT Treatment of biological material by pulsed electric fields is a versatile technique in biotechnology and biomedicine used, for example, in delivering DNA into cells (transfection), ablation of tumors, and food processing. Field exposure is associated with a membrane permeability increase usually ascribed to electroporation, i.e., formation of aqueous membrane pores. Knowledge of the underlying processes at the membrane level is predominantly built on theoretical considerations and molecular dynamics (MD) simulations. However, experimental data needed to monitor these processes with sufficient temporal resolution are scarce. The whole-cell patch-clamp technique was employed to investigate the effect of millisecond pulsed electric fields on DC-3F cells. Cellular membrane permeabilization was monitored by a conductance increase. For the first time, to our knowledge, it could be established experimentally that electroporation consists of two clearly separate processes: a rapid membrane poration (transient electroporation) that occurs while the membrane is depolarized or hyperpolarized to voltages beyond so-called threshold potentials (here, +201 mV and −231 mV, respectively) and is reversible within ~100 ms after the pulse, and a long-term, or persistent, permeabilization covering the whole voltage range. The latter prevailed after the pulse for at least 40 min, the postpulse time span tested experimentally. With mildly depolarizing or hyperpolarizing pulses just above threshold potentials, the two processes could be separated, since persistent (but not transient) permeabilization required repetitive pulse exposure. Conductance increased stepwise and gradually with depolarizing and hyperpolarizing pulses, respectively. Persistent permeabilization could also be elicited by single depolarizing/hyperpolarizing pulses of very high field strength. Experimental measurements of propidium iodide uptake provided evidence of a real membrane phenomenon, rather than a mere patch-clamp artifact. In short, the response of DC-3F cells to strong pulsed electric fields was separated into a transient electroporation and a persistent permeabilization. The latter dominates postpulse membrane properties but to date has not been addressed by electroporation theory or MD simulations.

INTRODUCTION

Exposure of cells to strong pulsed electric fields can induce a plethora of physiological effects. The current literature reflects a renewed interest in this subject, which has been studied, with varying intensity, since the 1970s (1,2). Meanwhile, this technique has been established as a versatile tool in various fields of biomedicine and biotechnology, including, among other things, gene therapy, cancer treatment, disinfection (e.g., of drugs and wounds), scarless healing of skin defects, decontamination of wastewater, and facilitated release of cellular ingredients from plant tissues (3–13). Depending on parameters such as pulse length (nanoseconds to milliseconds), frequency, field strength, and energy input, treatment of cells and tissues with electric fields can be employed even for contrasting purposes, such as stimulating cell proliferation and growth on the one hand (14) and induction of apoptosis on the other (15). Apparently, the molecular and cellular basis for the multitude of macroscopic effects is provided by different (and sometimes even opposing) processes triggered at the cellular level.

A primary target of strong electric pulses is always the plasma membrane. Usually, field exposure is associated with membrane charging and subsequent membrane permeabilization, which according to consensus can be explained by the formation of aqueous pores (i.e., electroporation; but see also Weaver and Chizmadzhev (16)). However, the time course and intensity of membrane permeability change during and after the pulse can be quite variable, which suggests that there is no simple, uniform mechanism underlying all the phenomena usually summarized under the label electroporation (17). Previously, we lacked efficient experimental strategies to separate and systematically unravel molecular processes induced by pulsed electric fields with precision and at sufficient temporal resolution.

These criteria are best met by the whole-cell configuration of the patch-clamp technique. Suitability of this experimental approach has recently been demonstrated by a series of publications dealing with Chinese hamster ovary cells (18,19) and protoplasts derived from tobacco culture cells (20–24). In those studies, electrical access to the cell interior was established by means of a fine-tipped patch electrode. Using the voltage-clamp mode, the membrane potential of tobacco protoplasts was driven to a sequence of well-defined voltages imposed homogenously over the entire membrane, and the current response of the cell was recorded. The transmembrane current density calculated as a function of voltage scales with pore formation and/or membrane

Submitted August 27, 2014, and accepted for publication January 29, 2015.
*Correspondence: lars.wegner@gmx.net
Editor: Hagan Bayley.

0006-3495/15/04/1660/12 $2.00
http://dx.doi.org/10.1016/j.bpj.2015.01.038

permeabilization per surface area. Whole-cell current-voltage relations obtained from these data allow, among other things, determination of the threshold potentials at which membrane permeabilization is initiated. Unfortunately, it is not possible to apply voltage pulses in the submillisecond time range, since it takes ~1 ms to charge the membrane to a predefined voltage. This could be considered a drawback of the technique, but there is evidence (e.g., from molecular dynamics simulations (25)) that results obtained with millisecond field exposure are also of relevance for shorter pulse lengths, even down to the nanosecond range, which currently receive much attention in the scientific community (26–32).

In light of the diversity of field effects on cells and tissues, we were interested in determining whether the characteristic features of membrane electroporation in tobacco cells, reported in the preceding studies, reflected general properties of biological membranes or were instead specific to tobacco cells. Previous work on mammalian cells (33–36), including several patch-clamp studies by Pakhomov and co-workers (28,37), provided evidence that postpulse membrane permeabilization prevailed for minutes, even up to hours, whereas in the tobacco culture cells, these long-term changes were less pronounced or even absent within the limits of accuracy (20). For this study, we selected a mammalian cell line, DC-3F, that has been established as a model system for studying electric field pulses as a tool in cancer treatment (electrochemotherapy) (30,38–40). Persistent permeabilization in this cell type could clearly be differentiated from the transient effect that occurred during pulse application, similar to previous reports on BY-2 tobacco cells (20–24).

MATERIALS AND METHODS

Biological material, cell culture and preparation of cells for patch-clamp experiments

The Chinese hamster lung cell line—DC-3F (41)—was grown in complete medium consisting of minimum essential medium with the addition of 10% fetal bovine serum and supplemented with antibiotics (500 U/mL penicillin, and 500 μg/mL streptomycin). The cells were maintained in a humidified atmosphere at 37°C and 5% CO_2. Cells were routinely subcultured every 2 days. All media and products for cell culture were purchased from Life Technologies (Regensburg, Germany).

For patch-clamp experiments, cells were trypsinized and resuspended in complete medium. Cells were then rinsed by centrifugation and resuspension in phosphate-buffered saline (14200 DPBS (Life Technologies), 2.7 mM KCl, 1.5 mM KH_2PO_4, 138 mM NaCl, and 8.1 mM Na_2HPO_4). Cells were then centrifuged once more and resuspended in the patch-clamp bath solution without calcium (see Electrophysiology, below). Cells were stored on ice.

Electrophysiology

Standard patch-clamp experiments were performed as described in detail previously (20–24). The setup used here was identical to that used in preceding studies. Micropipettes were fabricated from borosilicate glass (34500 99; Kimble, Rockwood, TN) with a two-step-procedure using a Narishige puller (PE-21, Narishige, Tokyo, Japan). Voltage was controlled and current recorded with an EPC-10 amplifier and using Patchmaster software (HEKA Electronics, Lambrecht, Germany). To calculate the actual transmembrane voltage drop from the applied command voltage at supraphysiological voltages, it was important to take the voltage drop at the access resistance into account, as described in previous publications. Briefly, when the voltage imposed by the amplifier was stepped by a certain value, ΔE_{clamp}, away from the holding potential (E_H), the fraction that actually dropped at the membrane ($E_M(t)$) could be calculated as a function of time using the equation (based on the assumption that $E_M \approx E_{clamp}$ at the holding potential)

$$E_M(t) = E_{clamp} - \big(I(t)/I_0\big)\Delta E_{clamp}, \quad (1)$$

where I(t) and I_0 are the recorded current response with time and the initial amplitude of the capacitive current spike, respectively. The latter is obtained by fitting an exponential relation to the time course of current relaxation upon imposing ΔE_{clamp}:

$$I_{cap}(t) = I_0 \exp(-t/\tau), \quad (2)$$

where $I_{cap}(t)$ is the capacitive current as a function of time and τ is the time constant of current relaxation. The validity of the approach was tested experimentally by measuring the voltage drop across the membrane with a voltage-sensitive fluorescent probe, ANNINE-6. Membrane potentials calculated according to Eq. 1 perfectly matched fluorescence intensities recorded in cells stained with this dye when both parameters were plotted as a function of E_{clamp} (23). The contribution of other resistances in series with the membrane and the pipette tip was negligible, as tested by dipping the very tip of the silver wire of the measuring electrode (without the glass micropipette) into the bath medium. The conductance exceeded that of pipette and porated membrane by more than two orders of magnitude (24). During a voltage pulse, no current decrease with time was observed that could have affected the outcome of the patch-clamp measurements, suggesting that electrode polarization was negligible.

Pipette solution was obtained by dissolving 120 mM KCl, 1 mM $CaCl_2$, 10 mM HEPES, 4 mM $MgCl_2$, and 10 mM EGTA. pH was adjusted to 7.2 by adding a small amount of KOH. Final osmolality was between 340 and 360 mOsmol kg^{-1}. Bath solution consisted of phosphate-buffered saline. Manitol was added to reach a final osmolality of 350 mOsmol kg^{-1}, pH 7.1. Unless stated otherwise, the solution was also supplemented with 0.1 mM $CaCl_2$. For this combination of solutions, a liquid junction potential of +2 mV was determined experimentally using Neher's method ((42); three independent experiments); this value was considered insignificant in the context of this study and therefore did not require any correction.

Verification of membrane permeabilization by propidium iodide staining

Membrane permeabilization of DC-3F cells was monitored by measuring propidium iodide (PI) uptake. To this end, the bath solution was supplemented with PI at a concentration of 30 μg/mL. For fluorescence imaging, we used the setup described previously (23). Briefly, fluorescence was elicited by exposing cells to light at a wavelength of 525 nm using a xenon lamp (Lambda DG-4plus, Sutter Instruments, Novato, CA). Light emitted by a cell was collected with a ProgRes MF^{cool} camera (Jenoptik, Jena, Germany). For imaging, we used a Brightline HC 525/50 excitation filter (AHF Analysentechnik, Tübingen, Germany), a FT 560 dichroic filter (Zeiss, Oberkochen, Germany), and a BP 575-640 emission filter (Zeiss). Data were recorded using an extended Patchmaster program kindly provided by HEKA electronics.

RESULTS

Electrophysiological properties of DC-3F cells under standard conditions

As a first step, experiments were performed with the aim of obtaining current-voltage relations of DC-3F cells in the physiological voltage range, i.e., to determine electrical features of the cellular membrane of nontreated cells. A literature screen did not provide any relevant information on this cell type, indicating that its electrical properties had not been characterized previously. To fill this gap, the whole-cell configuration of the patch-clamp technique was established, and the clamped membrane voltage was sequentially deflected to voltages ranging from −120 to +80 mV for 1.5 s (well below the threshold at which pore formation is induced). Between successive pulses, the membrane was held at 0 mV for 5 s. The current responses of the cell to pulses of varying amplitude were recorded and the current level after a 1.5-s pulse exposure was plotted against the clamped voltage, as shown in the three examples in Fig. 1. Current-voltage curves were linear (Fig. 1 *A*; 9 of 38 cells), inward-rectifying (Fig. 1 *B*; 17 of 38 cells), or S-shaped (Fig. 1 *C*; 12 of 38 cells). Experiments were performed either in the absence of Ca^{2+} or with 0.1 mM $CaCl_2$ added to the bath medium, without any obvious effect on the outcome. Since the small currents passing through the membrane at a given clamped voltage were frequently on the same order of magnitude as (or even lower than) leak currents by-passing the membrane due to an imperfect seal, the overall resistance often remained at a value close to 1 GΩ even after the whole-cell configuration was established. This made it hard to quantify the cellular membrane conductance using whole-cell patch-clamp experiments. Thus, conductance values calculated from the recorded IV curve represent an upper limit of the real membrane conductance (that would have been obtained after subtraction of the current passing the membrane-glass interface); values ranged from 0.018 to 0.375 nS/pF (Fig. 2).

Reversal potentials of current-voltage relations also varied widely, ranging from −45 to +2 mV. This could be interpreted in terms of a low-conductive, K^+-selective cellular membrane and a nonselective leak conductance (at least partly representing the seal) acting in parallel to a varying extent. The overall conductance tended to be lower when the reversal potential, E_{rev}, was closer to the Nernst potential of K^+, E_{K+} (−75 mV; Fig. 2). Based on this simple model, the K^+ conductance of the membrane, G_{K+}, is related to the total slope conductance recorded at E_{rev}, G_{total}, according to the equations

$$E_{rev} = \frac{G_{total} - G_{K+}}{G_{total}} E_{leak} + \frac{G_{K+}}{G_{total}} E_{K+} \quad (3)$$

and, provided that the reversal potential of the leak, E_{leak}, is 0 mV,

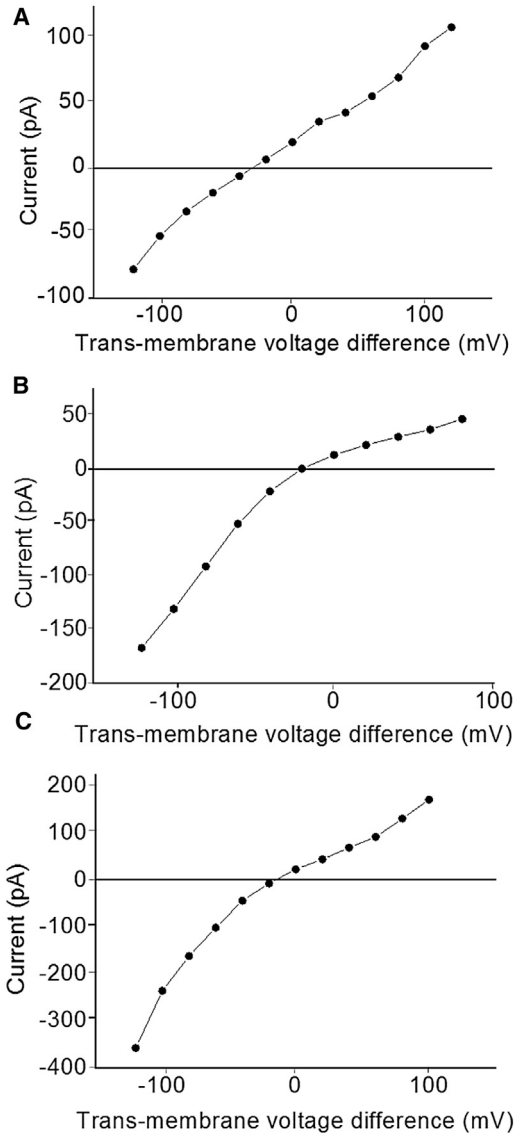

FIGURE 1 Three typical examples of current-voltage relations obtained for DC-3F cells by imposing a sequence of 1.5-s pulses covering the voltage range, as indicated in the figures; the clamped voltage was increased by increments of 20 mV per pulse, starting at −120 mV. Between successive pulses, the membrane was clamped at 0 mV for 5 s. Currents recorded at the end of each pulse were plotted against the respective clamped voltage. Current voltage relations were linear (*A*), inward rectifying (*B*), or S-shaped (*C*). Reversal potentials for the examples shown here were −30, −16, and −21 mV, respectively.

$$G_{total} = \frac{E_{K+}}{E_{rev}} G_{K+}. \quad (4)$$

However, the assumption that G_{K+} (normalized to the cell capacitance) is constant for all cells tested did not render an acceptable fit for the data set in Fig. 2 (data not shown). A more adequate description was found when G_{K+} was assumed to be linearly related to G_{total} ($G_{K+} = G_{K+,0} + m \times G_{total}$). We then end up with the empirical equation

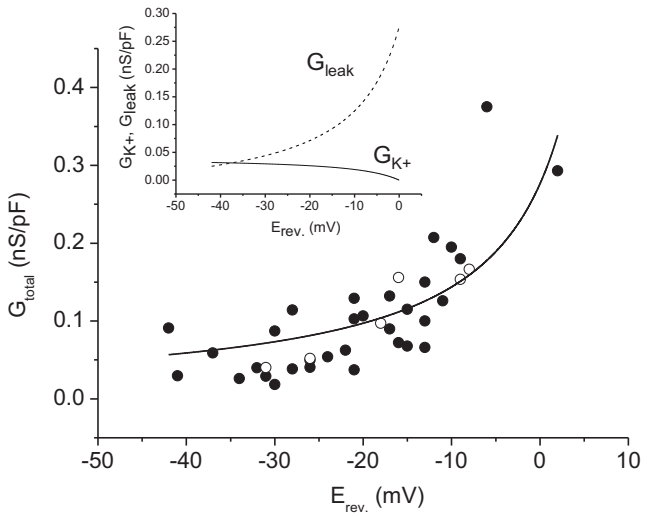

FIGURE 2 Plot of the recorded slope conductance at the reversal potential (G_{total}), divided by the cell capacitance to normalize for cell size, against the reversal potential, E_{rev}. Experiments were performed at 0.1 mM $CaCl_2$ in the bath (*solid symbols*) or in the absence of Ca^{2+} (*open symbols*). Data were fitted using Eq. 5 (*solid line*). Best-fit parameters were $G_{K,0} = 0.04$ nS/pF and $m = -0.144$. (*Inset*) Hypothetical dependence of G_{leak} (*dotted line*) and G_{K+} (*solid line*) on E_{rev} as calculated from Eqs. 3 and 5. For more details, see text.

$$G_{total} = \frac{G_{K+,0} \times E_{K+}}{E_{rev} - m \times E_{K+}}. \quad (5)$$

Fitting the data in Fig. 2 using Eq. 5 rendered a background K^+ conductance, $G_{K+,0}$, of 0.04 nS/pF and a value of -0.145 for the dimensionless factor m, indicating that an increase in leak conductance correlated with a decrease in G_{K+}, as depicted in the inset to Fig. 2. A more detailed analysis of putative K^+ transporters in the membranes of DC-3F cells was not attempted and is beyond the scope of this study. For studying membrane permeabilization by pulsed electric fields, our primary interest was that background currents carried by ion channels and electrogenic transporters were extremely low and not likely to interfere with field-induced pore formation. This is a definite advantage of using DC-3F cells over other cell lines (e.g., BY-2 protoplasts) for this type of investigation.

Electrical properties of DC-3F cells at supraphysiological voltages: short bipolar pulses of increasing magnitude

Subsequently, cells were challenged in the whole-cell configuration with a train of 10-ms pulses of alternating polarity. Intermittently, the voltage was clamped to 0 mV for at least 4 s. The magnitude was increased by increments of 40 mV from ±40 mV to final clamped voltages of ±280 or ±320 mV, respectively. These voltages were beyond the threshold of pore formation, as indicated by the current response recorded at slightly lower voltage amplitude (Fig. 3 *A*). The process of membrane charging was reflected by the initial capacitive-current spike. Capacitive current relaxed with an exponential time course until a relative current minimum was passed (Fig. 3 *A*, *inset*, *arrow*); subsequently, the current amplitude (positive or negative) increased again, then tended to level off at the end of the pulse. This second phase is due to field-induced membrane poration. At lower-voltage pulse amplitudes (Fig. 3 *B*), the capacitive current spike was superimposed on a very low steady-state background level. By plotting the current level at the end of the pulse against the respective transmembrane voltage (taking the access resistance into account; compare previous works (20,21,24)), a current-voltage relation could be obtained, as shown in Fig. 4. Note that two successive pulse trains rendered almost identical results, as in the majority of the experiments of this type ($n = 11$ of 15), indicating that this field treatment usually did not induce long-term effects. The slope of the current-voltage curve was low at intermediate voltages but increased strongly (by a factor of ~50) when the membrane was polarized beyond threshold voltages of −235 mV and +190 mV, respectively.

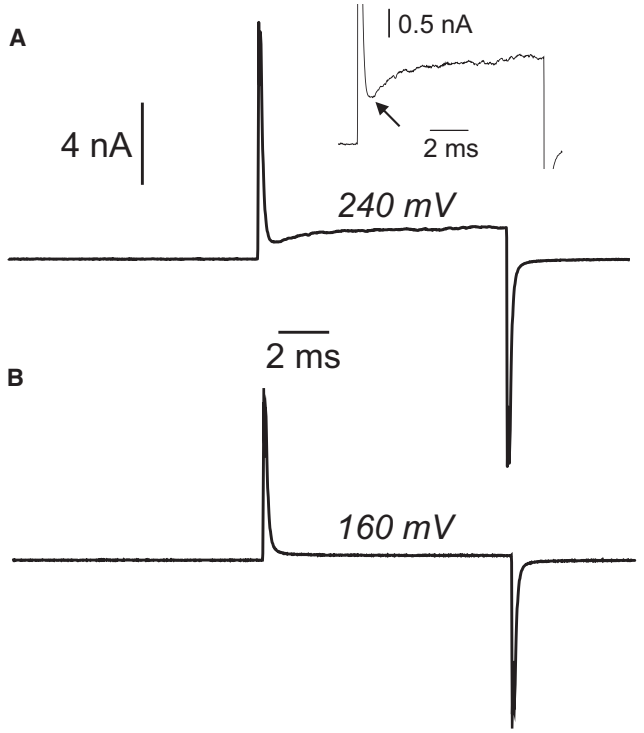

FIGURE 3 Two examples of current traces recorded on the same cell during administration of rectangular voltage pulses (command voltages are indicated in the figure). (*A*) The voltage step from 0 mV to 240 mV elicited a capacitive current spike and a subsequent slow conductive current increase. When the voltage was stepped back to the initial level after 10 ms, a negative-going capacitive current spike was elicited. (*Inset*) Detail of this trace at an enlarged scale. Arrow indicates the relative current minimum. (*B*) Current response to a 10-ms voltage pulse to 160 mV command voltage.

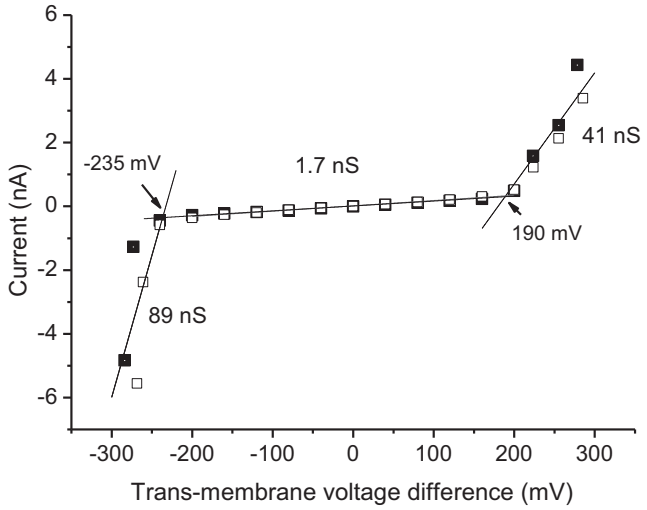

FIGURE 4 Current-voltage relations obtained from current responses to a series of 10-ms pulses, as shown in Fig. 3 (same experiment; *solid symbols*, first pulse sequence; *open symbols*, repetition of the experiment on the same cell after 17 s). The current level was measured at the end of each pulse and plotted against the transmembrane voltage difference calculated from command voltages (Eq. 1). Three segments of the curve could clearly be discerned for separate linear fitting of the slope conductances (*solid lines with conductance values*; linear relationships were fitted after pooling data points from successive sweeps). Intersection points of the linear fits mark the threshold potentials of pore formation (*arrows*); for this experiment, values of −235 mV and +190 mV were determined, as indicated in the figure.

On average, threshold potentials were −231 ± 8 mV and +201 ± 7 mV (data recorded in the presence of 0.1 mM Ca^{2+}, $n = 18$, and expressed as mean ± SE). In some of the experiments, it was not possible to extrapolate the threshold potential by fitting the slope of the current-voltage relations at hyperpolarization and depolarization, because only one or two data points were available for each. In these cases, we determined the voltage at which currents started to deviate significantly from the linear, low-background conductance. The threshold potential was defined as the arithmetic average of this value and the previous depolarizating and hyperpolarizing voltage step, respectively (that was obviously not yet supporting pore formation). A compilation of results obtained on DC-3F cells (Table 1) revealed close similarity with previous findings on BY-2 protoplasts (20–24), except that the threshold potentials were asymmetric in BY-2 protoplasts, and they were more or less symmetric in DC3-F cells, particularly in the absence of Ca^{2+} (−228 ± 13 and +224 ± 11 mV (mean ± SE), $n = 3$). Concurrent results, despite their very distant systematic provenance and cell-specific differences, e.g., in membrane composition (43), indicate that the phenomenon is common to all membranes. One reason for a slight asymmetry of threshold potentials depending on the extracellular Ca^{2+} concentration may be cellular surface charges (44) that are affected by Ca^{2+} binding.

TABLE 1 Comparison of DC-3F cells and BY-2 protoplasts with respect to the conductance increase induced by supraphysiological voltages

		DC-3F cells	Tobacco culture cells (BY-2)[a]
Threshold-potential (mV)	Depol	+201 ± 7 ($n = 18$)	+205 ± 14 ($n = 9$)
	Hyperpol	−231 ± 8 ($n = 18$)	−273 ± 16 ($n = 9$)
Conductance increase	Depol	8–100×	~56×
	Hyperpol	6–100×	~52×

Depol, depolarizing; Hyperpol, hyperpolarizing.
[a]Data from Wegner et al. (20).

During the first two pulse trains imposed on a DC-3F cell in the whole-cell configuration, membrane permeabilization was only observed at extremely negative or positive voltages. In the intermediate voltage range confined by well-defined threshold potentials, as demonstrated in Fig. 4, membrane conductance remained at a constant, very low level. After 10 ms of membrane polarization beyond the threshold values, the initial background conductance was rapidly restored when the voltage was returned to the physiological range, very similar to the case for BY-2 cells (22). This type of electroporation will therefore be termed transient. However, when the same protocol was imposed a third time, we observed a conductance increase by a factor of ~2 over the whole voltage range (including intermediate voltages), and the conductance increased even further during a fourth train (Fig. 5; same experiment as depicted in Fig. 4). Apparently, repetitive pulsing induced a sustained change of membrane properties that persisted even when voltages around 0 mV were reestablished. Therefore, this phenomenon is called persistent permeabilization. Note that during the third and fourth repetitions of the protocol, threshold potentials for transient poration remained more or less unchanged. Induction of persistent permeabilization, in addition to the transient one, was confirmed in four experiments conducted in the same way. During the fourth sweep, the membrane conductance in the intermediate range was always at least threefold higher than the initial value in all tested cells (see also further below for additional experiments on this issue).

To quantify the time required to restore the initial membrane conductance after a transient poration of the membrane, double-pulse protocols were applied. Transient electroporation was elicited by a 5-ms pulse to command voltages ranging from 280 to 360 mV. Subsequently, the voltage was stepped back to values ranging from 60 to 150 mV for 100 ms. Independent of pulse details that did not affect the outcome, pore closure was induced during this second voltage step. Subsequently, the membrane potential was returned to 0 mV. An example is shown in Fig. 6. Current relaxation during the second pulse segment followed a single-exponential time course; the best fit rendered a time constant of 19.9 ms, suggesting that the initial membrane conductance was restored after ~100 ms. On average,

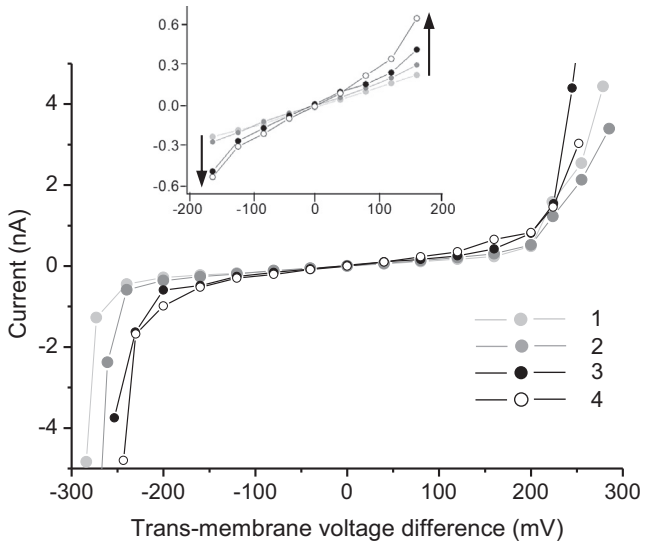

FIGURE 5 Current-voltage relations obtained in four successive runs (*shaded circles*; see key) of the same pulse protocol (same experiment as shown in Figs. 3 and 4). (*Inset*) Detail of the curve showing the shift in the slope of the current-voltage relation in the physiological voltage range with the third and fourth repeats of the same pulse sequence. The conductance increased at least twofold with respect to the first two sweeps. For more details, see the text

we obtained a time constant of 16.8 ± 2.8 ms (mean ± SE; $n = 5$). Care was taken to select only experiments where the initial membrane conductance was fully restored during this time, i.e., no persistent permeabilization interfered with the result.

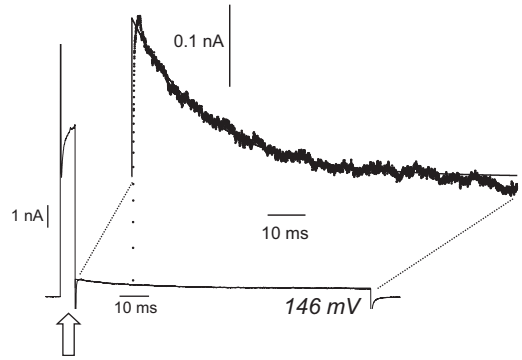

FIGURE 6 Time course of current relaxation after a 5-ms porating voltage pulse (*arrow*; command voltage, 360 mV; transmembrane voltage difference at the end of the pulse segment, 293 mV). Subsequent pore closure was monitored while clamping the voltage at 146 mV for 100 ms. The voltage was clamped to 0 mV both initially and at the end of the experiment. The complete current response to this double-pulse protocol is depicted for a representative experiment (three successive pulses were averaged; note that capacitive current spikes were truncated). The current relaxation during the second pulse segment is also shown at an enlarged scale. It was fitted with an equation of the form $I(t) = I_0 \exp(-(t - t_0)/\tau)$. The best fit (*solid line*) was obtained with a current amplitude, I_0, of 0.39 nA and a time constant, τ, of 19.9 ms. $t_0 = 15$ ms (start of second pulse segment).

The experimental approach that led to Fig. 5 revealed that a memory effect was apparently involved in the induction of persistent permeabilization. The cellular response to a certain pulse protocol depended strongly on the pretreatment history. This effect merited further attention.

Electrical properties of DC-3F cells at supraphysiological voltages: repetitive pulsing keeping the pulse amplitude constant

For a more detailed study of the memory effect, we used a double-pulse protocol similar to that imposed in Fig. 6. The membrane was repetitively depolarized to the same clamped voltage (ranging from 280 to 360 mV among different cells; $n = 8$). Results for two representative examples are depicted in Fig. 7, *A* and *B*. Pulse length was 10 ms; after each pulse, the clamped voltage was lowered to 80 mV for 25 or 100 ms and then returned to 0 mV and kept at this value for 5 s. The last voltage step and the respective current response (arrows at the enlarged details of the current races) were used to calculate the membrane resistance in the intermediate voltage range, which served as a measure to quantify persistent electropermeabilization. In the experiment shown in Fig. 7 *A*, the conductance increased stepwise at the third, fourth, and tenth pulses, whereas in Fig. 7 *B*, it was a one-step change (at pulse 15). In eight independent experiments, up to three levels of elevated conductance could be identified in addition to the background level (Fig. 7 *C*), indicating that distinct degrees of persistent permeabilization could be discerned. Note that conductance changes did not reflect a deterioration of the seal but resulted from a general increase in membrane permeability, as verified by monitoring uptake of the fluorescent dye PI (described in more detail below).

Interestingly, when the same type of experiment was repeated, but with the cell hyperpolarized instead of depolarized, changes in membrane conductance within a train of 20 pulses appeared to be more gradual (Fig. 8). No transition between distinct conductance levels was observed, indicating some asymmetrical polarity in this process for which there was no obvious explanation.

Persistent permeabilization by strong single pulses

Persistent permeabilization could also be induced by a single depolarizating or hyperpolarizing pulse of 5 or 10 ms duration when a more pronounced change in membrane potential was imposed (about ±400 mV or more). A representative example is shown in Fig. 9 *A*. Current-voltage relations in the physiological voltage range were acquired before and at several time intervals after this pulse, as depicted in Fig. 9 *B*, to assess possible changes in the shape of the IV curve and the reversal potential with time. Typically, current-voltage relations in the permeabilized state

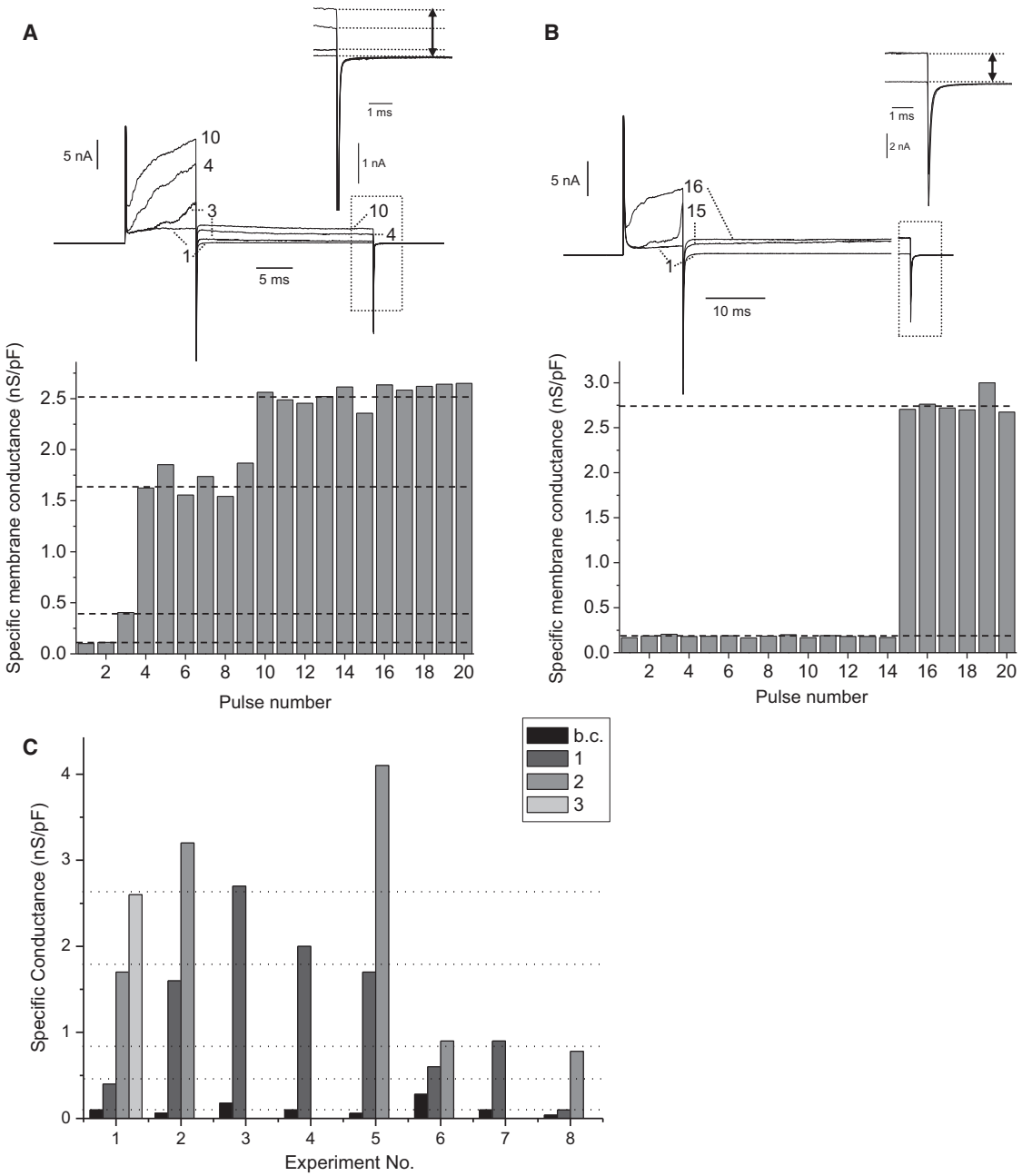

FIGURE 7 Two examples of the current response to repetitive application of a double-pulse protocol, consisting of a depolarization to 320 mV command voltage for 10 ms and successive clamp at 80 mV for 25 or 100 ms (*A* and *B*, *upper*; note that part of the trace is omitted in *B*). Subsequently, the membrane was stepped back to 0 mV for 5 s before the next pulse of the same type was applied. Individual repetitions are superimposed as indicated by numbers. The membrane conductance at the physiological voltage range was calculated from the difference in steady-state current level induced by a voltage step from 80 to 0 mV (redrawn at an enlarged scale in (*A*) and (*B*), as indicated by the arrows). Bar graphs (*A* and *B*, *lower*) show the conductance levels for the applied sequence of pulses. The conductance increased stepwise (*dotted lines*), either in several steps (*A*, *pulses 3*, *4*, and *10*) or in one step (*B*, *pulse 15*). These two examples were selected to reflect the variability among individual cells. (*C*) Summary of data for eight experiments carried out in the same way. Cells 1 and 3 correspond to the experiments shown in (*A*) and (*B*), respectively; in the other experiments, the same protocol was employed as in (*B*). Apparently, the distribution of conductances normalized to cell capacitance was non-Gaussian but reflected preferred conductance states of the membrane (*dotted lines*). b.c., background conductance.

were S-shaped directly after the strong pulse, and the curve flattened out with time after the pulse (Fig. 9 *B*). The conductance around 0 mV was more or less stable or decreased slightly (Fig. 9 *C*). In only a few cases did conductance increase strongly with time, as shown in Fig. 9 *D*; this example is likely to represent a case of irreversible electroporation leading to cell death (treated in more detail in the Discussion).

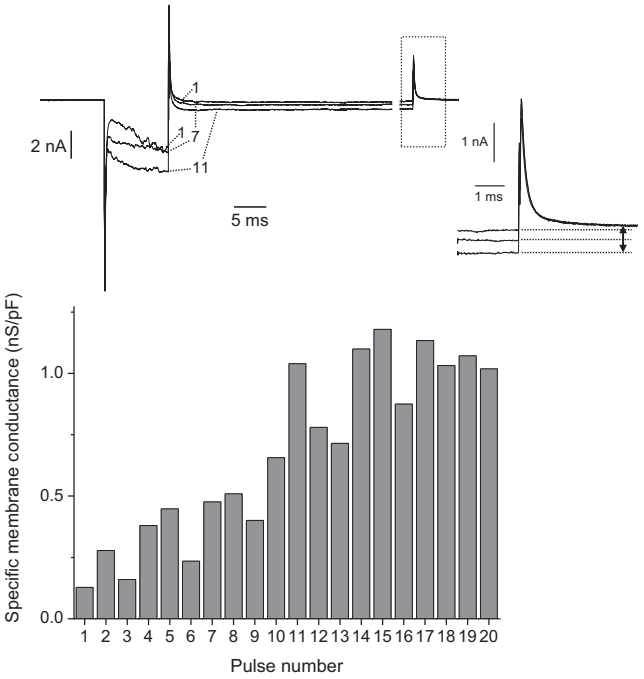

FIGURE 8 Current response to repetitive hyperpolarization exemplified by several superimposed current traces (*upper*). The same pulse sequence was used as in Fig. 7 *B*, but with opposite polarity. Note that membrane conductance calculated from current response to a voltage step from −80 to 0 mV increased gradually, in contrast to the result obtained with depolarization. A representative example from four qualitatively similar experiments is shown.

PI uptake studies confirm persistent membrane permeabilization by brief exposure to extreme voltages and are counterindicative of a patch-clamp artifact

The rather high conductance values associated with persistent membrane permeabilization needed additional experimental verification, because they could also have been attributed to a deterioration of the seal resistance due to repetitive pulsing. In the latter case, we would be dealing with a patch-clamp artifact rather than a true membrane phenomenon. Reversal potentials under these conditions were close to 0 mV (-2 ± 1 mV; $n = 18$) and were of little diagnostic value. To determine whether high conductance reflected membrane permeabilization or a patch-clamp artifact, whole-cell patch-clamp experiments were performed in the presence of 30 μg/mL PI in the bath. Fluorescence imaging is suitable for detecting pathways of PI diffusion into the cell at high spatial resolution, as demonstrated previously (28). In the experiments reported here, cells were challenged with a single strong depolarizing pulse of 10 ms duration and a voltage amplitude of ~400 mV that induced a maximum conductance increase in one step (Fig. 10). PI uptake was then monitored by recording the fluorescence signal. At 57 s, a local increase in fluorescence intensity was observed in the vicinity of the cellular membrane, but not close to the site where the pipette tip was inserted. By 44 s later, cytosolic fluorescence had increased more or less homogenously, and still no maximum was observed at the pipette-membrane interface, indicating that PI was getting into the cell not via this pathway but through the membrane. Only after ~5 min did a clear pattern of intensity start to evolve due to PI binding at the nucleus, which again did not coincide with the position of the pipette. These observations provide evidence that dye uptake was not due to a dramatic deterioration of the seal resistance. In three other independent experiments, our observations were very similar. These results further support the idea that the patch-clamp data reflect persistent permeabilization.

DISCUSSION

To our knowledge, this is the first detailed report on two distinct types of electroporation (or, rather, permeabilization) occurring in the same cell type. Remarkably, transient poration, which was detected during pulse application and relaxed within ~100 ms after the pulse, could be elicited separately from persistent poration by imposing few pulses to voltages just exceeding the threshold value. Separation of transient and persistent electroporation by choice of pulse parameters indicated that the two effects are triggered by separate mechanisms. This does not necessarily imply independence of the phenomena, but at least for transient poration, we can state that characteristic features such as threshold potential and membrane conductance in the porated state did not change even after the onset of persistent poration (Fig. 5).

Although there is no explicit report on the two types of poration in the literature, several hints, as well as seemingly contradictory results, provide circumstantial evidence. For example, experiments on electroporation of artificial bilayers showed that membrane conductance returned to the initial value within a few microseconds after the end of the pulse (45), and molecular dynamics simulations predicted pore closure even within nanoseconds (46). Still, cell uptake of fluorescent dyes or bleomycin was frequently observed even minutes after pulse application, indicating that the membrane was still in a permeabilized state. Weaver (47) therefore hypothesized the formation of what he called "complex, metastable pores" possibly involving "other components of the cell, e.g., cytoskeleton or tethered cytoplasmic molecules." In a study on in vivo tumor treatment in mice by trains of electric pulses, Ivorra and co-workers (48), using impedance spectroscopy, observed rapid relaxation of tissue conductivity (within ~100 ms) after each porating pulse, but the final conductance level exceeded the level after the preceding pulse, so that the steady-state tumor conductance increased stepwise and roughly doubled after the first 20 pulses (which the authors referred to as the "accumulative effect"). A similar effect had been reported

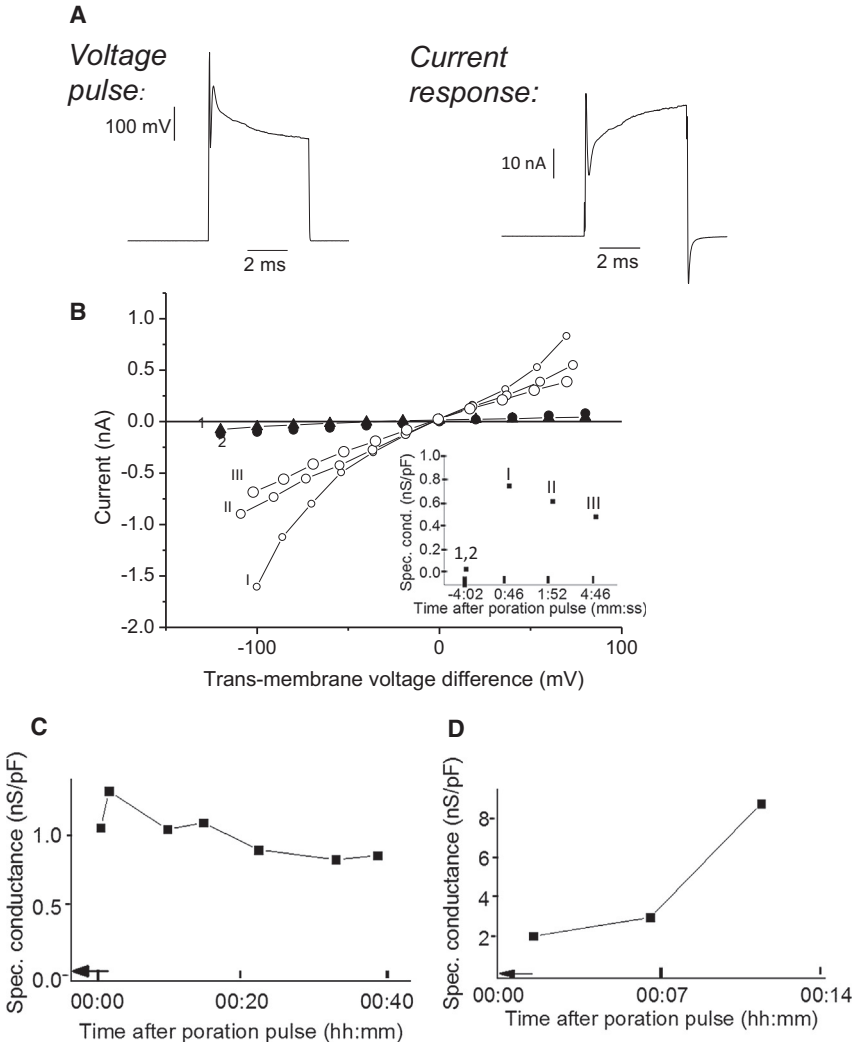

FIGURE 9 Persistent membrane permeabilization by a single, strong depolarizing pulse. (*A*) Time courses of transmembrane voltage drop and current response of the cell for the permeabilizing pulse (pulse length, 10 ms). (*B*) Current-voltage relations in the physiological voltage range obtained before (*solid symbols*; two repetitions) and at several times after the pulse (*open symbols*; see inset for the time course of the experiment). Note that the first current-voltage relation recorded after the permeabilizing pulse was S-shaped, but curves flattened out with time. (*C*) Long-term monitoring of membrane conductance at 0 mV (normalized to cell capacitance) for an experiment of the same type as shown in (*A*) and (*B*). Membrane conductance remained elevated for >40 min after the pulse but decreased slightly with time. (*D*) Similar experiment, but with progressive strong postpulse membrane conductance increase. Arrows indicate the conductance regime before application of the permeabilizing pulse (0.07 nS/pF in *C* and 0.1 nS/pF in *D*).

previously for the green alga *Valonia utricularis* (45), but that should be considered a special case because of its various structural peculiarities (49). Evidence for persistent permeabilization was also obtained in artificial membranes (45,50). Recently, a mathematical model of electroporation has been advanced that differentiates between short-term conductance and persistent permeability changes (51).

It is important to point out that the two types of electroporation reported here should not be equated with the well-known terms reversible and irreversible electroporation (52), which are based on the pragmatic criterion of cell survival after pulse treatment. Although irreversible electroporation has been attributed by some authors (e.g., Weaver (47)) to unrestricted growth of membrane pores, it is not necessarily associated with a certain membrane-bound process or mechanism. Irreversible electroporation could also result, for example, from apoptosis induced by Ca^{2+} influx into the cell. On the other hand, persistent electroporation (permeabilization) does not necessarily induce irreversible damage. For example, it has been shown that DC-3F cells remain viable even when the membrane is permeabilized for minutes after the pulse (53).

The term persistent electroporation/electropermeabilization is useful when comparing this phenomenon to transient poration but should be taken as a heading for a multifold phenomenon possibly arising from several membrane processes. Specific membrane conductance in this state ranged from 0.088 to 3.3 nS/pF, and current-voltage relations could be linear or (in the majority of the experiments, at least initially) S-shaped. Consistently, depolarizing pulses revealed the existence of several distinct persistent conductance states, whereas with hyperpolarization, the conductance increase was more gradual. Asymmetry of membrane responses to hyperpolarizing and depolarizing pulses may arise from nonuniform composition of the inner and outer leaflets of the membrane and a consequent difference in the density of fixed charges (44). Alternatively, it could be due to exposure of the anodic and cathodic sides of the membrane to solutions of different composition and/or to differences in the membrane curvature of the

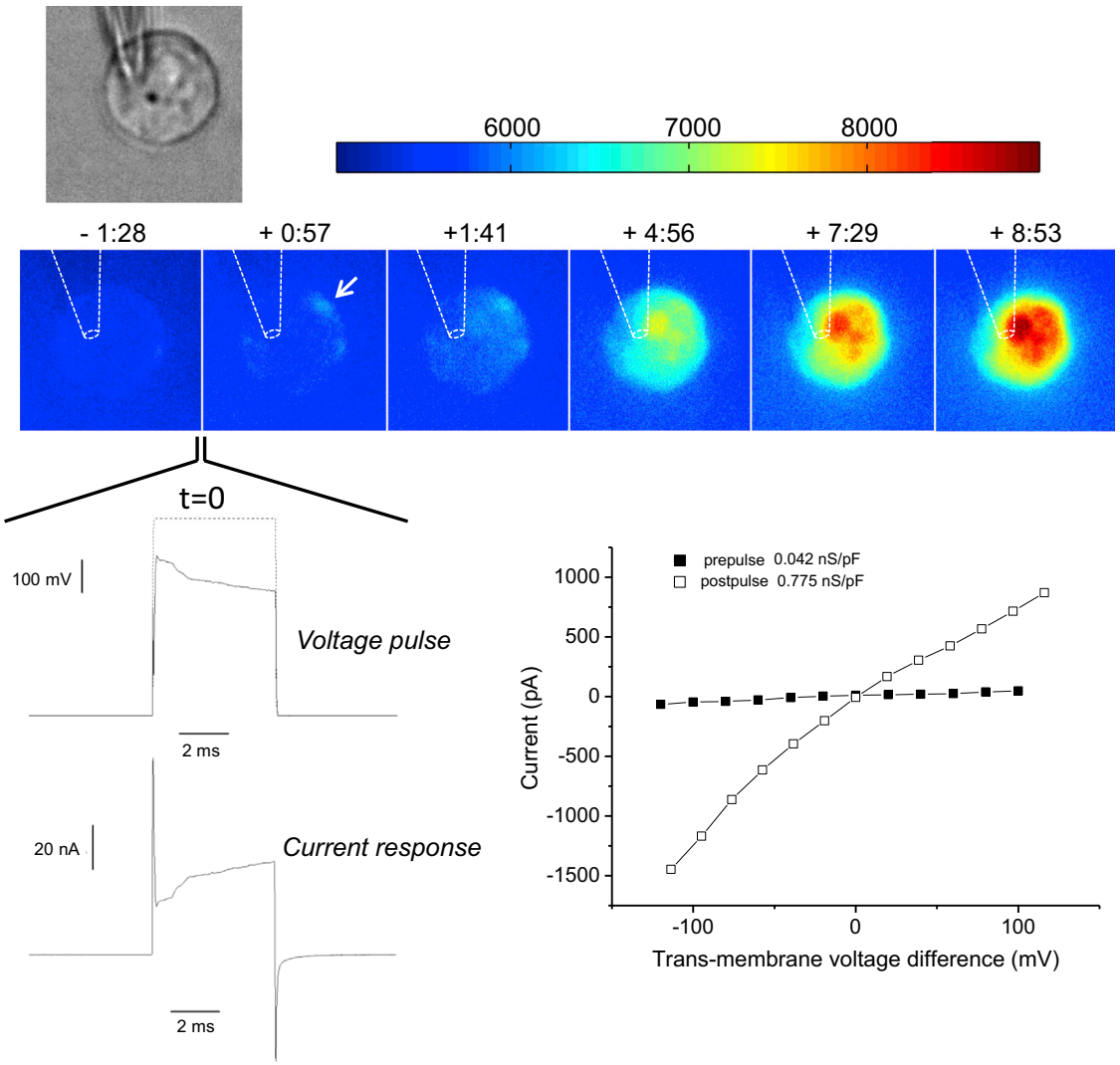

FIGURE 10 Testing seal integrity and membrane permeabilization by applying a strong, depolarizing pulse in the presence of PI in the bath. A sequence of images showing PI fluorescence before and at several time intervals after pulse application is shown. Time is given in minutes relative to pulse application. Fluorescence intensity is visualized by pseudocolors (see color scale at top, arbitrary units). The voltage pulse (*dotted line*, clamped voltage; *solid line*, actual transmembrane voltage drop) and the current response of the membrane are also depicted, as are current-voltage relations in the physiological voltage range before and after pulse application. Note that an elevated fluorescence level initially occurred in the vicinity of the membrane (*arrow*), but not where the pipette (*dotted lines*) was attached. Apparently, PI did not enter the cell because of poor contact between membrane and glass (i.e., a bad seal) or membrane damage at the contact site of the pipette. Spots of high fluorescence intensity coinciding with the position of the nucleus started to appear after a delay of ~5 min. See text for more details. To see this figure in color, go online.

two sides with respect to the electrical gradient. At present, however, there is no direct clue to the cause of the disparate response in this particular case. Clearly, additional work is required to characterize persistent electropermeabilization in more detail and to unravel the underlying molecular mechanism(s). Transient electroporation, on the other hand, seems to be represented well by classical electroporation theory, with formation of initially hydrophobic membrane pores that turn into a hydrophilic electrically conductive state with lipid headgroups lining the pore (47,54).

An interesting phenomenon associated with persistent electropermeabilization is the pronounced memory effect of its appearance in successive pulses at voltages around 300 mV (Figs. 5 and 7). Apparently, the treatment history of the cell had a strong influence on its response to a pulse. A plausible explanation is that a change in membrane properties, most likely of a chemical nature, is induced by the administration of an electric field pulse. This modification is not (fully) reversible during the interpulse period and tends to accumulate until a threshold is reached that leads to a stepwise or gradual increase in membrane conductance over the whole voltage range.

Membrane permeabilization by pulsed electric fields is generally believed to be associated primarily with changes of the lipid structure occurring both in biological

membranes and protein-free artificial lipid bilayers. In contrast, controlled passage of ions into and out of the cell in the physiological context is thought to be mediated by membrane-spanning proteins, especially by ion channels that form stable, hydrophilic membrane pores. However, in light of recent results, a clear separation of the two phenomena appears to be questionable and somewhat arbitrary. Field-induced membrane pores can be highly cation-selective (21) and display a nonlinear conductance (this article), features typically ascribed to ion channels. Transition from a nonporated to a porated state can even be described adequately with a Boltzmann distribution closely resembling that used to characterize ion channel gating (24). On the other hand, it was recently demonstrated that membrane-spanning proteins are not required to induce stepwise changes in membrane conductance usually associated with ion channel activity (55), indicating that those pores were, at least partly, lined by lipids. Consistent with those results, Heimburg and co-workers suggest an alternative mechanism of controlled passage of ions through membranes that is based on a local phase transition of the lipid bilayer mediated by membrane proteins (56). Further convergence of concepts for membrane transport enforced by electric pulses on the one hand and physiological membrane transport on the other may take place in the near future, facilitated by the use of the patch-clamp technique to study both phenomena.

Even though the patch-clamp technique proved to be a valuable tool in studying effects of pulsed electric fields on cellular membranes in unprecedented detail, the fact that the pulse length could not be reduced to the submillisecond range is a limitation of this technique. However, a comparison of current-voltage curves after the administration of nanosecond pulses indicates that pulse length by itself had little impact on postpulse permeability, even though side effects related to temperature increase, local changes in pH, and formation of reactive oxygen species at the membrane are expected to be more pronounced during millisecond pulses. Either nanosecond field exposure (at very high field strengths!) affects at least one of these secondary factors (e.g., reactive oxygen species production) to such an extent that persistent permeabilization is already triggered, or these side effects are of minor importance only for the membrane response to field exposure.

Molecular dynamics simulation consistently predicted good agreement of results over the whole timescale of pulse lengths usually applied (25). Therefore, there is good reason to assume that results presented here are also relevant for shorter pulse lengths.

In conclusion, it is established in this report that what is generally called electroporation consists of (at least) two distinct processes, a transient poration in the presence of the electric field and long-term changes in membrane permeability. The latter effect is likely to be most important for applied aspects such as introduction of macromolecules into the cell interior. The data presented here were obtained on a single cell line, DC-3F, which proved to be an excellent model system for studying (for example) the cellular uptake of membrane-impermeable drugs like bleomycin. Therefore, our results are likely representative of similar processes in other cell lines (even if persistent poration is less pronounced or completely lacking in individual cells, as observed for BY-2 cells). Future work on a broader spectrum of cell types will be required to unravel the molecular mechanism by which short-term pulse exposure is transduced into long-term changes in membrane properties.

ACKNOWLEDGMENTS

We thank Sarah Rocke, Karlsruhe, for her help with DC-3F cell culture and Dr. Lluis Mir and Isabelle Leray, Paris, France, for providing us with the cells. We also acknowledge valuable discussions on basic mechanisms within the framework of COST TD1104.

REFERENCES

1. Neumann, E., and K. Rosenheck. 1972. Permeability changes induced by electric impulses in vesicular membranes. *J. Membr. Biol.* 10: 279–290.
2. Zimmermann, U., G. Pilwat, and F. Riemann. 1974. Dielectric breakdown of cell membranes. *Biophys. J.* 14:881–899.
3. Mir, L. M., J. Gehl, …, M. Marty. 2006. Electrochemotherapy—an easy, highly effective and safe treatment of cutaneous and subcutaneous metastases: results of ESOPE (European standard operating procedures of electrochemotherapy) study. *EJC Suppl.* 4:3–13.
4. Andre, F. M., and L. M. Mir. 2010. Nucleic acids electrotransfer in vivo: mechanisms and practical aspects. *Curr. Gene Ther.* 10:267–280.
5. Breton, M., and L. M. Mir. 2011. Microsecond and nanosecond electric pulses in cancer treatments. *Bioelectromagnetics.* 33:106–123.
6. Golberg, A., G. F. Broelsch, …, M. L. Yarmush. 2014. Eradication of multidrug-resistant *A. baumannii* in burn wounds by antiseptic pulsed electric field. *Technology* (*Singap. World Sci.*). 2:153–160.
7. Golberg, A., G. F. Broelsch, …, M. L. Yarmush. 2013. Non-thermal, pulsed electric field cell ablation: a novel tool for regenerative medicine and scarless skin regeneration. *Technology* (*Singap. World Sci.*). 1:1–8.
8. Yarmush, M. L., A. Golberg, …, D. Miklavčič. 2014. Electroporation-based technologies for medicine: principles, applications, and challenges. *Annu. Rev. Biomed. Eng.* 16:295–320.
9. Gusbeth, C., W. Frey, …, H. Bluhm. 2009. Pulsed electric field treatment for bacteria reduction and its impact on hospital wastewater. *Chemosphere.* 75:228–233.
10. Donsì, F., G. Ferrari, and G. Pataro. 2010. Applications of pulsed electric field treatments for the enhancement of mass transfer from vegetable tissue. *Food Eng. Rev.* 2:109–130.
11. Sack, M., C. Schultheiss, and H. Bluhm. 2005. Triggered Marx generators for the industrial-scale electroporation of sugar beets. *IEEE Trans. Ind. Appl.* 41:707–714.
12. Eing, C., M. Goettel, …, W. Frey. 2013. Pulsed electric field treatment of microalgae—benefits for microalgae biomass processing. *IEEE Trans. Plasma Sci.* 41:2901–2907.
13. Goettel, M., C. Eing, …, W. Frey. 2013. Pulsed electric field assisted extraction of intracellular valuables from microalgae. *Algal Res.* 2:401–408.
14. Eing, C., S. Bonnet, …, W. Frey. 2009. Effects of nanosecond pulsed electric field exposure on *Arabidopsis thaliana*. *IEEE Trans. Dielectr. Electr. Insul.* 16:1322–1328.

15. Hofmann, F., H. Ohnimus, …, C. Jassoy. 1999. Electric field pulses can induce apoptosis. *J. Membr. Biol.* 169:103–109.

16. Weaver, J. C., and Y. A. Chizmadzhev. 1996. Theory of electroporation: a review. *Bioelectrochem. Bioenerg.* 41:135–160.

17. Teissie, J., M. Golzio, and M. P. Rols. 2005. Mechanisms of cell membrane electropermeabilization: a minireview of our present (lack of?) knowledge. *Biochim. Biophys. Acta.* 1724:270–280.

18. Pliquett, U., H. Krassen, …, K. Schoenbach. 2005. Asymmetric changes in membrane conductance due to hyper-and depolarization: probing with current and voltage clamp. *Proc. Int. Fed. Med. Biol. Eng.* 11:1924–1929.

19. Krassen, H., U. Pliquett, and E. Neumann. 2007. Nonlinear current-voltage relationship of the plasma membrane of single CHO cells. *Bioelectrochemistry.* 70:71–77.

20. Wegner, L. H., B. Flickinger, …, P. Nick. 2011. A patch clamp study on the electro-permeabilization of higher plant cells: Supra-physiological voltages induce a high-conductance, K^+ selective state of the plasma membrane. *Biochim. Biophys. Acta.* 1808:1728–1736.

21. Wegner, L. H. 2013. Cation selectivity of the plasma membrane of tobacco protoplasts in the electroporated state. *Biochim. Biophys. Acta.* 1828:1973–1981.

22. Wegner, L. H., and S. Schönwälder. 2012. Electroporation of plant cells studied with the patch clamp technique. *Proc. Euro-Asian Puls. Power Conf. Int. Conf. High-Power Part. Beams.*

23. Wegner, L. H., W. Frey, and S. Schönwälder. 2013. A critical evaluation of whole cell patch clamp studies on electroporation using the voltage sensitive dye ANNINE-6. *Bioelectrochemistry.* 92:42–46.

24. Wegner, L. H. 2015. The conductance of cellular membranes at supra-physiological voltages. *Bioelectrochemistry.* 103:34–38.

25. Delemotte, L., and M. Tarek. 2012. Molecular dynamics simulations of lipid membrane electroporation. *J. Membr. Biol.* 245:531–543.

26. Vernier, P. T., Y. Sun, …, M. A. Gundersen. 2003. Calcium bursts induced by nanosecond electric pulses. *Biochem. Biophys. Res. Commun.* 310:286–295.

27. Vernier, P. T., Y. Sun, …, M. A. Gundersen. 2004. Nanoelectropulse-induced phosphatidylserine translocation. *Biophys. J.* 86:4040–4048.

28. Pakhomov, A. G., A. M. Bowman, …, K. H. Schoenbach. 2009. Lipid nanopores can form a stable, ion channel-like conduction pathway in cell membrane. *Biochem. Biophys. Res. Commun.* 385:181–186.

29. Nesin, O. M., O. N. Pakhomova, …, A. G. Pakhomov. 2011. Manipulation of cell volume and membrane pore comparison following single cell permeabilization with 60- and 600-ns electric pulses. *Biochim. Biophys. Acta.* 1808:792–801.

30. Silve, A., and L. M. Mir. 2011. Cell electropermeabilization and cellular uptake of small molecules: the electrochemotherapy concept. *In* Clinical Aspects of Electroporation. S. T. Kee, J. Gehl, and E. W. Lee, editors. Springer, New York, pp. 69–82.

31. Breton, M., L. Delemotte, …, M. Tarek. 2012. Transport of siRNA through lipid membranes driven by nanosecond electric pulses: an experimental and computational study. *J. Am. Chem. Soc.* 134: 13938–13941.

32. Vernier, P. T., Y. Sun, and M. A. Gundersen. 2006. Nanoelectropulse-driven membrane perturbation and small molecule permeabilization. *BMC Cell Biol.* 7:37.

33. Rols, M. P., and J. Teissié. 1990. Electropermeabilization of mammalian cells. Quantitative analysis of the phenomenon. *Biophys. J.* 58:1089–1098.

34. Rols, M. P., C. Delteil, …, J. Teissié. 1998. Control by ATP and ADP of voltage-induced mammalian-cell-membrane permeabilization, gene transfer and resulting expression. *Eur. J. Biochem.* 254:382–388.

35. Teissié, J., and C. Ramos. 1998. Correlation between electric field pulse induced long-lived permeabilization and fusogenicity in cell membranes. *Biophys. J.* 74:1889–1898.

36. Pucihar, G., T. Kotnik, …, J. Teissié. 2008. Kinetics of transmembrane transport of small molecules into electropermeabilized cells. *Biophys. J.* 95:2837–2848.

37. André, F. M., M. A. Rassokhin, …, A. G. Pakhomov. 2010. Gadolinium blocks membrane permeabilization induced by nanosecond electric pulses and reduces cell death. *Bioelectrochemistry.* 79:95–100.

38. Orlowski, S., J. Belehradek, Jr., …, L. M. Mir. 1988. Transient electropermeabilization of cells in culture. Increase of the cytotoxicity of anticancer drugs. *Biochem. Pharmacol.* 37:4727–4733.

39. Poddevin, B., S. Orlowski, …, L. M. Mir. 1991. Very high cytotoxicity of bleomycin introduced into the cytosol of cells in culture. *Biochem. Pharmacol.* 42 (*Suppl*):S67–S75.

40. Tounekti, O., G. Pron, …, L. M. Mir. 1993. Bleomycin, an apoptosis-mimetic drug that induces two types of cell death depending on the number of molecules internalized. *Cancer Res.* 53:5462–5469.

41. Biedler, J. L., and H. Riehm. 1970. Cellular resistance to actinomycin D in Chinese hamster cells in vitro: cross-resistance, radioautographic, and cytogenetic studies. *Cancer Res.* 30:1174–1184.

42. Neher, E. 1992. Correction for liquid junction potentials in patch clamp experiments. *Methods Enzymol.* 207:123–131.

43. Martin, S. W., B. J. Glover, and J. M. Davies. 2005. Lipid microdomains—plant membranes get organized. *Trends Plant Sci.* 10:263–265.

44. Golberg, A., C. S. Rae, and B. Rubinsky. 2012. *Listeria monocytogenes* cell wall constituents charge effect on irreversible electroporation threshold. *Biochim. Biophy.s Acta.* 1818:689–694.

45. Benz, R., and U. Zimmermann. 1980. Relaxation studies on cell membranes and lipid bilayers in the high electric field range. *J. Electroanal. Chem. Interfacial Electrochem.* 116:723–739.

46. Tarek, M. 2005. Membrane electroporation: a molecular dynamics simulation. *Biophys. J.* 88:4045–4053.

47. Weaver, J. C. 1995. Electroporation theory. Concepts and mechanisms. *Methods Mol. Biol.* 47:1–26.

48. Ivorra, A., B. Al-Sakere, …, L. M. Mir. 2009. In vivo electrical conductivity measurements during and after tumor electroporation: conductivity changes reflect the treatment outcome. *Phys. Med. Biol.* 54:5949–5963.

49. Heidecker, M., S. Mimietz, …, U. Zimmermann. 2003. Structural peculiarities dominate the turgor pressure response of the marine alga *Valonia utricularis* upon osmotic challenges. *J. Membr. Biol.* 192: 123–139.

50. Cranfield, C. G., B. A. Cornell, …, B. Martinac. 2014. Transient potential gradients and impedance measures of tethered bilayer lipid membranes: pore-forming peptide insertion and the effect of electroporation. *Biophys. J.* 106:182–189.

51. Leguèbe, M., A. Silve, …, C. Poignard. 2014. Conducting and permeable states of cell membrane submitted to high voltage pulses: mathematical and numerical studies validated by the experiments. *J. Theor. Biol.* 360:83–94.

52. Ivorra, A., and B. Rubinsky. 2010. Historical review of irreversible electroporation in medicine. *In* Irreversible Electroporation. B. Rubinsky, editor. Springer, Berlin/Heidelberg, pp. 1–21.

53. Puc, M., T. Kotnik, …, D. Miklavčič. 2003. Quantitative model of small molecules uptake after in vitro cell electropermeabilization. *Bioelectrochemistry.* 60:1–10.

54. Krassowska, W., and P. D. Filev. 2007. Modeling electroporation in a single cell. *Biophys. J.* 92:404–417.

55. Stoddart, D., M. Ayub, …, H. Bayley. 2014. Functional truncated membrane pores. *Proc. Natl. Acad. Sci. USA.* 111:2425–2430. http://dx.doi.org/10.1073/pnas.1312976111.

56. Heimburg, T. 2010. Lipid ion channels. *Biophys. Chem.* 150:2–22.